



Chinese Pharmaceutical Association  
Institute of Materia Medica, Chinese Academy of Medical Sciences

Acta Pharmaceutica Sinica B

[www.elsevier.com/locate/apsb](http://www.elsevier.com/locate/apsb)  
[www.sciencedirect.com](http://www.sciencedirect.com)



ORIGINAL ARTICLE

# Molecular characterization and structure basis of a malonyltransferase with both substrate promiscuity and catalytic regiospecificity from *Cistanche tubulosa*



Xiao Liu<sup>a,\*</sup>, Yuyu Liu<sup>a,b,#</sup>, Xiping Xu<sup>a,b</sup>, Wenqian Huang<sup>a,b</sup>,  
Yaru Yan<sup>a,b</sup>, Yingxia Wang<sup>a,b</sup>, Weisheng Tian<sup>a,b</sup>, Ting Mo<sup>a,b</sup>,  
Xiaoxue Cui<sup>a,b</sup>, Jun Li<sup>a,b,\*</sup>, She-Po Shi<sup>a,\*</sup>, Pengfei Tu<sup>a,\*</sup>

<sup>a</sup>Modern Research Center for Traditional Chinese Medicine, Beijing Research Institute of Chinese Medicine, Beijing University of Chinese Medicine, Beijing 100029, China

<sup>b</sup>Modern Research Center for Traditional Chinese Medicine, School of Chinese Materia Medica, Beijing University of Chinese Medicine, Beijing 100029, China

Received 11 December 2023; received in revised form 24 January 2024; accepted 4 February 2024

## KEY WORDS

Plant acyltransferase;  
Malonyltransferase;  
Malonylated glycosides;  
Enzymatic catalysis;  
Enzyme promiscuity

**Abstract** Enzymatic malonylation of natural glycosides provides a promising alternative method for drug-like malonylated glycosides supply. However, the catalytic potential and structural basis of plant malonyltransferase are far from being fully elucidated. This work identified a new malonyltransferase CtMaT1 from *Cistanche tubulosa*. It displayed unprecedented mono- and/or di-malonylation activity toward diverse glycosides with different aglycons. A “one-pot” system by CtMaT1 and a malonyl-CoA synthetase was established to biosynthesize nine new malonylated glycosides. Structural investigations revealed that CtMaT1 possesses an adequately spacious acyl-acceptor pocket capable of accommodating diverse glycosides. Additionally, it recognizes malonyl-CoA through strong electrostatic and hydrogen interactions. QM/MM calculation revealed the H167-mediated S<sub>N</sub>2 reaction mechanism of CtMaT1, while dynamic simulations detected the formation of stable hydrogen bonds between the glucose-6-OH group and H167, resulting in its high malonylation regiospecificity. Calculated energy profiles of two isomeric glycosides highlighted lower reaction energy barriers towards glycoside substrates, emphasizing CtMaT1's preference for glycosides. Furthermore, a mutant CtMaT1<sub>H36A</sub> with notably increased

\*Corresponding authors.

E-mail addresses: [fcliuxiao@163.com](mailto:fcliuxiao@163.com) (Xiao Liu), [drj666@163.com](mailto:drj666@163.com) (Jun Li), [shishepo@163.com](mailto:shishepo@163.com) (She-Po Shi), [pengfeitu@163.com](mailto:pengfeitu@163.com) (Pengfei Tu).

<sup>#</sup>Present address: Department of Microbial Chemistry, Beijing Key Laboratory of Antimicrobial Agents, Institute of Medicinal Biotechnology, Chinese Academy of Medical Sciences, Peking Union Medical College, Beijing 100050, China.

Peer review under the responsibility of Chinese Pharmaceutical Association and Institute of Materia Medica, Chinese Academy of Medical Sciences.

<https://doi.org/10.1016/j.apsb.2024.02.007>

2211-3835 © 2024 The Authors. Published by Elsevier B.V. on behalf of Chinese Pharmaceutical Association and Institute of Materia Medica, Chinese Academy of Medical Sciences. This is an open access article under the CC BY-NC-ND license (<http://creativecommons.org/licenses/by-nc-nd/4.0/>).

di-malonylation activity was obtained. The underlying molecular mechanism was illuminated through MM/GBSA binding free energy calculation. This study significantly advances the understanding of plant acyltransferases from both functional and protein structural perspectives, while also providing a versatile tool for enzymatic malonylation applications in pharmacology.

© 2024 The Authors. Published by Elsevier B.V. on behalf of Chinese Pharmaceutical Association and Institute of Materia Medica, Chinese Academy of Medical Sciences. This is an open access article under the CC BY-NC-ND license (<http://creativecommons.org/licenses/by-nc-nd/4.0/>).

## 1. Introduction

Natural glycosides are a reliable source of drug leads<sup>1,2</sup>. The sugar moieties of these compounds usually exist as conjugates, typically in their acylated forms (acetyl, coumaroyl, caffeoyl, feruloyl, etc.). Such conjugations are significantly beneficial to their pharmaceutical uses<sup>3</sup>. Malonylation is one of the most common forms of aliphatic acylation in nature. Malonyl residue substituted on the sugar moiety is important for stabilizing labile structures<sup>4,5</sup>, changing lipophilicities<sup>6</sup>, protecting the glycosyl moiety from enzymatic degradation, and detoxifying xenobiotics or biogenic compounds<sup>7–10</sup>.

Recently, malonylated glycosides have attracted more and more attention in plant physiology and drug discovery due to their important physiological functions<sup>7,11–14</sup> and desired druggability<sup>15–18</sup>. Some of the representative bioactive malonylated glycosides are shown in Fig. 1A. However, the time-consuming and high costs of extraction and isolation from natural materials largely limit their availabilities. On the other hand, the selective chemical acylation on sugar units is hindered because of the poor specificity and unpredictability of the products<sup>21,22</sup>. By contrast, acylation reaction catalyzed by glycoside acyltransferase can be an alternative due to its high catalytic efficiency, regioselectivity, mild reaction conditions, and controllable processes<sup>23,24</sup>.

In plants, acylation of secondary metabolites is catalyzed by a family of acyl-CoA dependent acyltransferases, named BAHD superfamily enzymes after the first four biochemically characterized enzymes of the group. To date, hundreds of BAHD acyltransferases have been characterized and systematically reviewed by D'Auria<sup>19</sup>, Bontpart et al.<sup>20</sup>, and Wang et al.<sup>25</sup>. A large number of them were identified as malonyltransferases. They mainly use malonyl-CoA (MLC) as an acyl-donor to perform transacylation reactions in a variety of aromatic compounds. Anthocyanins and flavonoids were the most reported acyl-acceptors of malonyltransferases as summarized in Supporting Information Table S1. It was reported that malonyltransferases usually have strict substrate specificities corresponding to the substrates found or expected to be present in the mother plant<sup>4,26</sup>. The catalysis specificity of plant acyltransferases hampers their extensive enzymatic synthesis applications to some extent.

*Cistanche tubulosa* is a traditional medicinal herb that is abundant with phenylethanoid glycosides (PhGs) whose glycoside cores are often decorated with diverse acyl substituents, such as acetyl, coumaroyl, caffeoyl, feruloyl, vanilloyl, and syringoyl groups (Supporting Information Fig. S1)<sup>27</sup>. In this article, in an attempt to explore new glycoside acyltransferases with novel activities for enzymatic acylation applications, a new malonyltransferase, CtMaT1, was amplified from *C. tubulosa*. Functional characterization revealed the unprecedented substrate promiscuity of CtMaT1 towards diverse glycosides and its high catalysis

regiospecificity at the 6-OH position of glucose moiety. The structural basis of the unique catalysis characteristics of CtMaT1 was further explored. Key residues involved in the malonylation process and the recognition of both acyl-donor and acceptors were identified. A mutant showing enhanced di-malonylation activity was generated and the underlying molecular mechanism was also elucidated.

## 2. Materials and methods

### 2.1. Plant materials and chemicals

*C. tubulosa* was collected from Xinjiang Uygur Autonomous Region. Substrates for extensive enzyme assays were purchased from Push Biotechnology (Chengdu, China) and Biopurify Phytochemicals (Chengdu, China). Other reagents were purchased from Sigma–Aldrich (Darmstadt, Germany) unless specifically addressed.

### 2.2. Gene clone and heterologous expression of CtMaT1 and MatB

Total RNA was extracted using an OMEGA Plant RNA Extraction Kit. Full-length of *CtMaT1* was amplified using the Clontech RACE Kit. The coding sequence of *CtMaT1* was cloned from *C. tubulosa* cDNA using primers shown in Supporting Information Table S2 with *EcoR* I and *Not* I as restriction sites. The *MatB* gene was amplified from the cDNA of *Arabidopsis thaliana* using primers with *BamH* I and *Sal* I as restriction sites. DNA amplicons were digested and inserted into pET-28a vector. Obtained recombinant plasmid was then transformed into *Escherichia coli* Transetta DE3 and confirmed by sequencing. Recombinant strains' culture conditions and fusion protein purification procedures were the same as reported previously<sup>28</sup>.

### 2.3. Phylogenetic analysis of CtMaT1

Alignment of sequences was generated using ClustalW. The neighbor-joining phylogenetic tree was drawn using MEGA version 10.2 software<sup>29</sup>. Numbers at the nodes indicate percent bootstrap values. The reliability of the tree was measured by bootstrap analysis with 1000 replicates.

### 2.4. Assays for acylation activity and substrate specificity of CtMaT1

The standard enzymatic assays were performed in a 150  $\mu$ L mixture containing 0.8 mmol/L acyl-donor, 0.4 mmol/L acyl-acceptor, 1 mmol/L DTT, and 20  $\mu$ g of purified CtMaT1 in

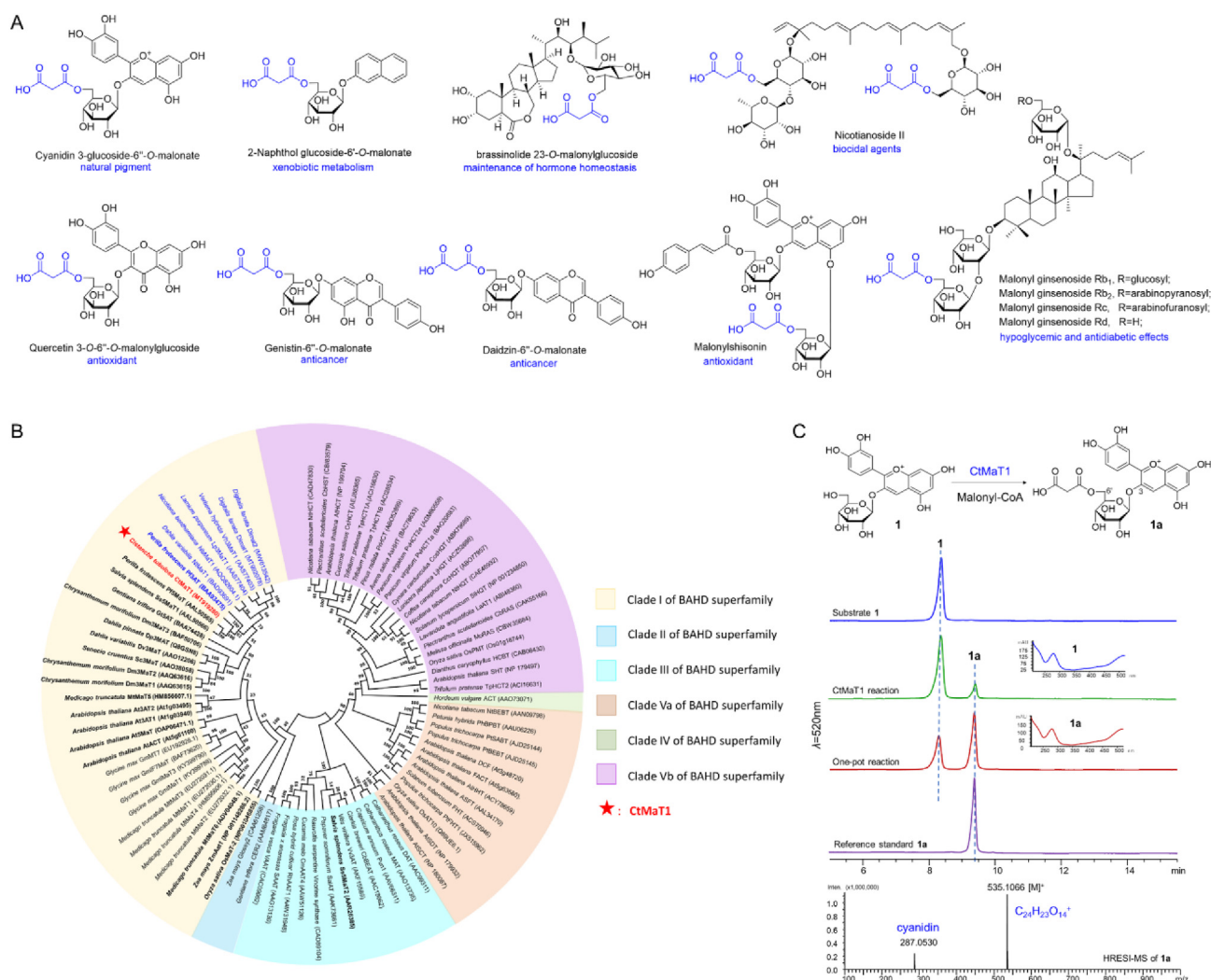


**Figure 1** Phylogenetic analysis and functional identification of a new acyltransferase CtMaT1. (A) Representative bioactive malonyl glycosides. (B) Phylogenetic analysis of CtMaT1 with other acyltransferases belonging to the BAHD family. All listed BAHD acyltransferases are classified into different clades (I–IV, Va, and Vb) and subgroups based on reviews by D’Auria<sup>19</sup> and Bontpart et al.<sup>20</sup> Clade I (yellow background) consist of BAHD family members that are involved in the modification of phenolic glucosides, predominantly AATs. Two enzymes Glossy2 and CER2, involved in the extension of long-chain epicuticular waxes, belong to clade II (blue background). The majority of members within clade III (cyan background) accept a diverse range of alcohol substrates, and these acyltransferases are mainly involved in the modification of alkaloid compounds or volatile ester biosynthesis. An agmatine coumaroyltransferase ACT in barley located in clade IV (green background). BAHD members present in clade V can be subdivided into several subgroups. Clade Va (orange background) includes the “BAHD benzoyltransferases subgroup” and “alkyl-hydroxycinnamate ester BAHD-acyltransferases subgroup”. Clade Vb (purple background) mainly includes the hydroxycinnamoyl-CoA: shikimate/quininate hydroxy-cinnamoyltransferases (HCT) and hydroxy-cinnamoyl-CoA: quinate hydroxy-cinnamoyltransferases (HQT), and their relatives. All characterized AATs were shown in bold characters. CtMaT1 is located in Clade I and is labeled with a red star. (C) HPLC chromatogram, UV spectra, and HRESI-MS spectra of the malonylation reaction of cyanidin 3-glucoside (**1**) by CtMaT1.

100 mmol/L potassium phosphate buffer (pH 6.0). The reactions were incubated for 12 h at 30 °C, and terminated by adding a double volume of ice-cold methanol. The precipitated proteins were removed by centrifugation at 15,000 rpm for 30 min, and the supernatants were concentrated by vacuum concentration. Residues were re-dissolved in 200  $\mu$ L methanol and centrifuged at 12,000 rpm at 4 °C for 30 min. The obtained supernatants were subjected to HPLC and HRESI-MS analyses as described in Supporting Information Method S1.

### 2.5. Biochemical properties and kinetic parameters determination of CtMaT1

To investigate the enzymatic properties of CtMaT1, the effects of different reaction times, pH values, temperatures, and divalent metal ions on the activity of CtMaT1 were studied as described in Supporting Information Method S2.

For kinetic studies of CtMaT1, enzymatic assays were performed in a final volume of 100  $\mu$ L containing 100 mmol/L

potassium phosphate buffer (pH 6.0), 1 mmol/L DTT, 2 mmol/L malonyl-CoA, 9.9  $\mu\text{g}$ /1.4  $\mu\text{g}$  of purified CtMaT1, and varying concentrations (25–2000  $\mu\text{mol/L}$ ) of 1/2. The reactions were conducted at 30 °C for 45 min/20 min, terminated with 200  $\mu\text{L}$  of ice-cold MeOH, and centrifuged at 15,000 $\times g$  for 30 min. Supernatants were analyzed by analytical reverse-phase HPLC. The kinetic parameters including the Michaelis–Menten constant ( $K_m$ ) and  $V_{\text{max}}$  were calculated by nonlinear regression analysis using GraphPad Prism 7 software.

## 2.6. *Agrobacterium-mediated transient expression and subcellular localization of CtMaT1 in Nicotiana benthamiana*

Transient expression and subcellular localization of CtMaT1 were both performed in *N. benthamiana* leaves or protoplasts through agroinfiltration using pCAMBIA1300 35s-EGFP binary vector and pBWA(V)HS vector, respectively, as described in [Supporting Information Methods S3, S4](#).

## 2.7. *Enzymatic synthesis of malonyl-CoA and methylmalonyl-CoA*

The acyl-donor (malonyl-CoA and methylmalonyl-CoA) were enzymatically synthesized by MatB<sup>30</sup> using the malonic acid and methylmalonic acid as substrate, respectively. The reaction mixture consisted of 1.5 mmol/L CoA, 3 mmol/L malonic acid (methylmalonic acid), 1 mmol/L DTT, 3 mmol/L ATP, and 5 mmol/L MgCl<sub>2</sub> in 100 mmol/L potassium phosphate (pH 6.0, 150  $\mu\text{L}$ ). The reaction was initiated by adding 15  $\mu\text{g}$  of purified MatB protein. After incubation at 30 °C for 12 h, the reaction was terminated by the addition of 4% (*w/v*) ammonium acetate. Reaction mixtures were then filtered and the supernatants were analyzed by a TOSOH TSKgel ODS Column (4.6 mm I.D.  $\times$  250 mm, 5  $\mu\text{m}$ ) using the mobile phase of solvent A (0.5 % trifluoroacetic acid) and solvent B (acetonitrile) at 1.0 mL/min with a gradient elution procedure as follows: A:B (*v/v*): 0 min (100:0)–5 min (100:0)–35 min (60:40)–38 min (40:60)–43 min (0:100). Peaks were measured at 257 nm.

## 2.8. *Construction of the one-pot reaction system*

The one-pot reaction system consisted of 0.4 mmol/L malonyl acceptors, 6 mmol/L ATP, 3 mmol/L CoA, 6 mmol/L malonic acid (methylmalonic acid), 2 mmol/L DTT, and 10 mmol/L MgCl<sub>2</sub> in 150  $\mu\text{L}$  potassium phosphate reaction buffer (100 mmol/L, pH 6.0) with the purified 75  $\mu\text{g}$  MatB and 20  $\mu\text{g}$  CtMaT1. After incubation at 30 °C for 12 h, the reaction was terminated by adding 300  $\mu\text{L}$  of methanol. The sample preparation and LC–MS analysis procedures were the same as described above.

## 2.9. *Preparation of malonylated glycosides by CtMaT1*

Glycoside substrates were dissolved in dimethyl sulfoxide (DMSO). The preparative–scale reaction systems were maintained in 100 mmol/L potassium phosphate reaction buffer (pH 6.0) by 15 mg MatB protein, 4 mg CtMaT1 protein together with 0.02 mmol malonyl acceptors (compounds **2**, **6**, **7**, **12**, **21**, **22**, **24** and **25**, respectively), 0.2 mmol malonic acid, 0.1 mmol acetyl-CoA, 0.2 mmol ATP, 10 mmol/L MgCl<sub>2</sub> and 2 mmol/L DTT. The reactions were incubated at 30 °C for 12 h. The obtained

solution was filtered and the supernatant was submitted to chromatography using a macroporous resin column. Aliquots including the targeted product were combined and further purified by semi-preparative HPLC to obtain **2a**, **6a**, **7a**, **12a**, **21a**, **22a**, **24a**, **25a**, and **25b**. 1D- and 2D-NMR data of prepared malonylated glycosides were summarized in [Supporting Information](#).

## 2.10. *AlphaFold2 structure prediction, molecular docking, and electrostatic potential calculation*

The structure model of CtMaT1 was predicted by AlphaFold2<sup>31</sup>. The reasonability of the model was evaluated by Ramachandran plot, PROCHECK analysis, and SAVES tools<sup>32</sup>. Molecular docking studies of CtMaT1 with different substrates were accomplished by AutoDock Vina<sup>33</sup>. Ligands were pre-processed with proper charges and hydrogen atoms using AutoDock Tools 1.5.7. The probable binding pockets of MLC and acyl-acceptor were aligned from the templates of 2E1T and 5KJW, respectively. The grid box was set as 60  $\times$  60  $\times$  60 Å with a 0.375 Å spacing. The optimum docking complex with the best binding affinity was chosen to identify the key residues surrounding the substrate in a distance  $\leq 4$  Å. Graphical manipulation of the docking results was performed using PYMOL software.

Protein electrostatic potential was calculated using the adaptive Poisson–Boltzmann solver (APBS) tool. A potential scale from  $-5$  to  $+5$  KT/e was employed in PYMOL software. Electrostatic charges of MLC atoms were calculated by using the Gaussian 09 at the B3LYP/6-311G(d,p) level<sup>34</sup>.

## 2.11. *Dynamic simulation, MM/GBSA predicted binding free energy calculation and decomposition*

Molecular dynamics (MD) simulations were performed using the Amber20 software package. The Amber ff19SB force field was applied for the protein<sup>35</sup>. Molecular structures of the natural product ligands were optimized by the B3LYP/6-311G(d) method<sup>36,37</sup>. Substrate parameters were generated using the antechamber module and general AMBER force field (GAFF)2 with RESP charges<sup>38</sup>. The structure was immersed into a truncated octahedral box that extended 10 Å away from the solute border, using the TIP3P water model and periodic boundary conditions<sup>39</sup>. Fourteen Na<sup>+</sup> ions (for substrates **2**, **6**, **7**, **12**, **21**–**23**, **25**, and **28**) or fifteen Na<sup>+</sup> ions (for substrate **25a**) were added into the box to neutralize the system for CtMaT1–MLC–substrate complex. Subsequent dynamic simulations were performed as reported previously<sup>28</sup>.

The total substrate binding free energies and the energy decomposition of each residue were computed utilizing the Molecular Mechanics/Generalized Born Surface Area (MM/GBSA) methodology with MMGBSA.py program<sup>40</sup> implemented in AMBER20 using the last 10 ns dynamic simulation trajectories.  $\Delta G_{\text{bind}}$  is calculated based on Eq. (1)

$$\Delta G_{\text{bind}} = \Delta G_{\text{vdw}} + \Delta G_{\text{ele}} + \Delta G_{\text{polar}} + \Delta G_{\text{nonpolar}} - T\Delta S \quad (1)$$

The terms  $\Delta G_{\text{vdw}}$  and  $\Delta G_{\text{ele}}$  represent the van der Waals and electrostatic energy contributions in the gas phase.  $\Delta G_{\text{polar}}$  and  $\Delta G_{\text{nonpolar}}$  indicate the polar and nonpolar solvent interaction energies, respectively. The calculation of  $T\Delta S$  via normal mode analysis was deemed impractical due to its time-consuming in large systems and high margin of error, resulting in the value

being disregarded. The last 10 ns simulation trajectories were extracted to calculate the binding free energy with an interval of 40 ps.

### 2.12. QM/MM calculation

The geometry optimization and density functional theory (DFT) chemical description for the molecular structures of all title compounds were performed using the Gaussian09 program<sup>41</sup> package with M062X<sup>37,42</sup> for all atoms. We optimized all structures in the present work by the quantum mechanics/molecular mechanics (QM/MM) method in the Gaussian 09 program. The QM region consisting of MU-Glu or MU-Gal, MLC, and the surrounding key residues were described by DFT method M062X at 6-311G\*\* basis set, while the MM atoms from other residues were simulated by the UFF force field<sup>43</sup>. The zero-point energy (ZPE) and BSSE correction were calculated by 6-311++G\*\* basis set based on the M062X theory level. Harmonic vibration frequency calculations were performed for all stationary points to confirm them as local minima (zero imaginary frequencies).

### 2.13. Mutants construction, enzymatic assays, and structure analysis

The mutants of CtMaT1 were constructed using the Transgen Biotech Fast Mutagenesis system using primers listed in Supporting Information Table S2. Subsequent protein expression and functional identification procedures were the same as that of CtMaT1 aforementioned. The protein structure of CtMaT1<sub>H36A</sub> was predicted by AlphaFold2. MLC was imported into CtMaT1<sub>H36A</sub> mutant *via* superimposition based on the conformation of MLC in the wild type of CtMaT1. The substrate docking process was the same with CtMaT1 as described above.

### 2.14. DPPH radical scavenging assay

All tested compounds were dissolved in DMSO at a final concentration of 50  $\mu\text{mol/L}$ , and mixed with a DPPH solution (100  $\mu\text{mol/L}$ ). 50  $\mu\text{mol/L}$  Trolox and solution without compound were used as the positive and negative control, respectively. All tests were performed in triplicate in 96-well microplates. After incubation at 30 °C for 1 h, absorbances at 515 nm were measured. The radical scavenging activities were calculated using Eq. (2) and expressed as percent inhibition.

$$\text{Inhibition (\%)} = (1 - \text{Sample OD}_{515 \text{ nm}} / \text{control OD}_{515 \text{ nm}}) \times 100 \quad (2)$$

## 3. Results and discussion

### 3.1. Identification of a new anthocyanin malonyltransferase CtMaT1 from *C. tubulosa*

To probe new acyltransferase genes in *C. tubulosa*, we initially analyzed the transcriptome of *C. tubulosa* based on annotations of assembly sequences. The full length of a new BAHD acyltransferase gene, *CtMaT1*, was cloned from *C. tubulosa* cDNA using primers in Table S2 through the RACE method (Supporting Information Fig. S2). The obtained sequence was 1979 bp long with an ORF of 1347 bp (GenBank accession MT919280). The

deduced protein sequence blast found that the conserved H $\times\times\times$ D motif and DFGWG motif of the BAHD acyltransferase superfamily<sup>44</sup>, as well as another specific YFGNC motif belonging to the anthocyanin acyltransferase (AAT) family all present in CtMaT1 (Supporting Information Fig. S3). Phylogenetic analysis of CtMaT1 with currently identified BAHD family acyltransferases found that CtMaT1 was phylogenetically closely related to several acyltransferases which had been reported to display certain substrate tolerance (shown in blue characters in Fig. 1B), such as Pf3AT (accepting seven anthocyanins)<sup>45</sup>, NtMaT1 (accepting anthocyanin, flavonol, and naphthol glucosides)<sup>46</sup>, NbMat1 (accepting several aromatic glycosides)<sup>47</sup>, Vh3MAT1 & Lp3MAT1 (accepting anthocyanin and flavonols)<sup>48</sup>, and D1mat1 & D1mat2 (accepting various hydroxypregnanes)<sup>49</sup>. These observations implied the potential versatility of CtMaT1, which prompted us to investigate its substrate tolerance and potential applications in enzyme catalysis. *CtMaT1* was subsequently expressed in *E. coli* to obtain the recombinant protein through Ni-chelating affinity chromatography purification (Supporting Information Fig. S4) in a protein yield of 5.0 mg/L.

To functionally identify CtMaT1, cyanidin 3-glucoside (**1**), a commonly occurring anthocyanin, was utilized as the initial acyl-acceptor. In the presence of MLC, a product (**1a**) was detected in the assay through HPLC analysis (Fig. 1C). The high-resolution electrospray ionization mass spectrometry (HRESI-MS) spectrum of **1a** exhibited a characteristic mass spectrometry of malonylated anthocyanins with an [M]<sup>+</sup> ion at  $m/z$  535.1066 (calcd. for C<sub>24</sub>H<sub>23</sub>O<sub>14</sub><sup>+</sup> 535.1082) and a fragment ion at  $m/z$  287.0530 (corresponding to cyanidin)<sup>50</sup>. The structure of **1a** was fully identified as cyanidin-3-(6'-malonylglucoside) by comparing it with the authentic reference standard, indicating that the malonyl group was transferred to the C6-glycosyl hydroxy group. CtMaT1 was further expressed in *N. benthamiana* leaves through agroinfiltration. With the addition of **1** and MLC, a product was accumulated and detected through HPLC and HRESI-MS analyses with the same retention time and mass spectrum compared with **1a** in *in vitro* reaction (Supporting Information Fig. S5), which confirmed the activity of CtMaT1 as an AAT. Nevertheless, no products were observed in the reactions using other acyl-donors including acetyl-CoA, caffeoyl-CoA, coumaroyl-CoA, and feruloyl-CoA, which indicated the high acyl-donor specificity of CtMaT1 toward MLC.

### 3.2. Malonylation of salidroside by CtMaT1, and kinetic study and subcellular localization of CtMaT1

To assess the acylation capability of CtMaT1 towards other glycosides, salidroside (**2**), a key intermediate in the biosynthetic pathway of PhGs in *C. tubulosa* was employed as the acceptor substrate. When MLC was utilized as the acyl-donor, a conspicuous product **2a** was observed (Fig. 2A). HRESI-MS analysis found a [M-H]<sup>-</sup> of **2a** at  $m/z$  385.1127 (calcd. for C<sub>17</sub>H<sub>21</sub>O<sub>10</sub> 385.1140). A fragment ion at  $m/z$  341.1227 [M-H-CO<sub>2</sub>]<sup>-</sup> was also observed (Fig. 2A). These observations provide evidence for the occurrence of malonylation at **2** and suggest the versatility of CtMaT1 in catalyzing this modification.

The biochemical properties of CtMaT1 were further investigated. The optimum reaction pH value and temperature of CtMaT1 were determined to be pH 6.0 (100 mmol/L KH<sub>2</sub>PO<sub>4</sub>-K<sub>2</sub>HPO<sub>4</sub>) and 30 °C, respectively. The conversion yield increased linearly within 1 h and reached the highest yield after

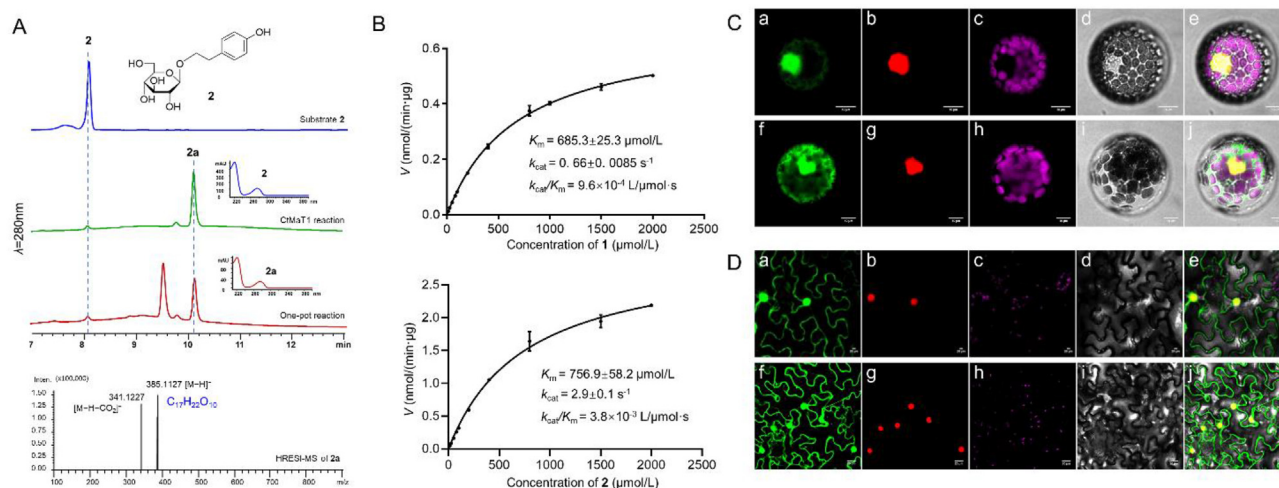


**Figure 2** Malonylation of salidroside (**2**) by CtMaT1 and kinetic study and subcellular localization investigations of CtMaT1. (A) HPLC-UV and HRESI-MS spectra of the malonylation reaction of **2** by CtMaT1. (B) Kinetic study ( $K_m$ ,  $k_{cat}$ , and  $k_{cat}/K_m$ ) of CtMaT1 using MLC as acyl-donor, **1** and **2** as acyl-acceptors, respectively. (C–D) Subcellular localization investigation of CtMaT1 in *N. benthamiana* protoplasts (C, Scale bar 10  $\mu\text{m}$ ) and leaves (D, Scale bar 20  $\mu\text{m}$ ) using nls-mKATE as a nucleus marker. (a–e) Fluorescence field image of GFP-CtMaT1 (a), nucleus marker (b), chloroplast (c), bright field image (d), merge of a–d (e); (f–j) Fluorescence field image of free GFP as control. Fluorescence field image of free GFP (f), nucleus marker (g), chloroplast (h), bright field image (i), merge of (f–i) (j).

5 h. The enzyme activity was found to be independent of divalent metal ions (Supporting Information Fig. S6). Kinetic studies of CtMaT1 were also performed using **1** and **2** as acyl-acceptors, respectively (Fig. 2B). Their  $K_m$  values were calculated as  $685.3 \pm 25.3 \mu\text{mol/L}$  (for **1**) and  $756.9 \pm 58.2 \mu\text{mol/L}$  (for **2**), respectively. The result indicated that CtMaT1 showed comparable catalysis affinity towards both anthocyanin and other glycosides.

As far as we know, CtMaT1 is the first acyltransferase capable of catalyzing malonylation of PhGs. However, no malonylated PhGs have been detected in *C. tubulosa* to date. To address this issue, subcellular localization analysis was conducted on CtMaT1 through transient expression of GFP-CtMaT1 fusion protein in both *N. benthamiana* protoplasts (Fig. 2C) and leaves (Fig. 2D). GFP-CtMaT1 signals were co-localized with the nucleus marker nls-mKATE which contains a specific nucleus-localized leader peptide (MDPKKKRKV). The result suggested that GFP-CtMaT1 is a kind of nucleus-localized malonyltransferase that is distinct from the cytosol or endoplasmic reticulum localization commonly observed in enzymes involved in the biosynthesis pathway of PhGs such as glycosyltransferases<sup>51</sup>. Additionally, RT-PCR analysis revealed high expression of CtMaT1 in flowers, while PhGs in *C. tubulosa* are predominantly distributed in the underground parts (Supporting Information Fig. S7). Furthermore, considering salidroside's role as a key intermediate for echinacoside biosynthesis, it was predicted that the differential tissue-specific expression patterns and subcellular compartmentalization of CtMaT1 and key enzymes in the PhGs biosynthesis pathway results in the production of PhGs lacking malonyl substitutions in *C. tubulosa*.

### 3.3. CtMaT1 displayed unprecedented substrate promiscuity towards diverse glycosides with different aglycon skeleton

To further explore the acyl-acceptor tolerance of CtMaT1, an acceptor library comprising 84 structurally diverse substrates with

various scaffolds that are found in natural products was employed. It consists of different kinds of aglycons (listed in Supporting Information Fig. S8 and Table S3) and their glycoside derivatives (listed in Fig. 3 and Supporting Information Table S4). All reaction mixtures were processed and subjected to HPLC-UV and HRESI-MS analyses (Supporting Information Figs. S9–S47). Surprisingly, CtMaT1 displayed unprecedented substrate promiscuity by catalyzing the malonylation of all tested glycoside compounds, including anthocyanin glycosides (**1**), phenylethanoid glycosides (**2,3**), stilbene glycosides (**4,5**), naphthol glycoside (**6**), anthraquinone glycoside (**7**), flavone glycosides (**8,9**), flavonone glycosides (**10,11**), flavonol glycosides (**12–14**), isoflavone glycosides (**15–20**, **30–31**), xanthone glycoside (**21**), coumarin glycosides (**22–24**), lignan glycoside (**25**), iridoid glycosides (**26,27**), diterpenoid glycoside (**28**), cyanophoric glycoside (**29**), chalcone glycoside (**32**), and triterpenoid saponins (**33–41**). Interestingly, although CtMaT1 could catalyze the malonylation of many glycoside compounds (Fig. 3 and Supporting Information Table S5), their corresponding aglycons could not be accepted by CtMaT1, which indicated that CtMaT1 shows high selectivity towards glycoside substrate and the sugar moiety is crucial for the activity of CtMaT1.

Enzyme promiscuity has received considerable attention during the past decade. Many promiscuous cases have been discovered in different kinds of enzymes, such as glycosyltransferases<sup>52,53</sup>, prenyltransferases<sup>54</sup>, cytochrome P450 enzymes<sup>55</sup>, and SAM-dependent enzymes<sup>56</sup>. However, most of the known AATs, even a majority of the reported BAHD acyltransferase members, display substrate selectivity mainly toward anthocyanins and phenolic compounds (Table S1)<sup>19,20</sup>. For CtMaT1, its substrate scope not only covers frequently reported phenolic glycosides including a variety of flavonoid glycosides and coumarin glycosides, but also a diverse range of other glycoside classes including terpenoid glycosides, phenylethanoid glycosides, stilbene glycosides, anthraquinone glycoside, xanthone glycoside, lignan glycoside, and cyanophoric glycoside (Fig. 3). To the best of our knowledge, CtMaT1

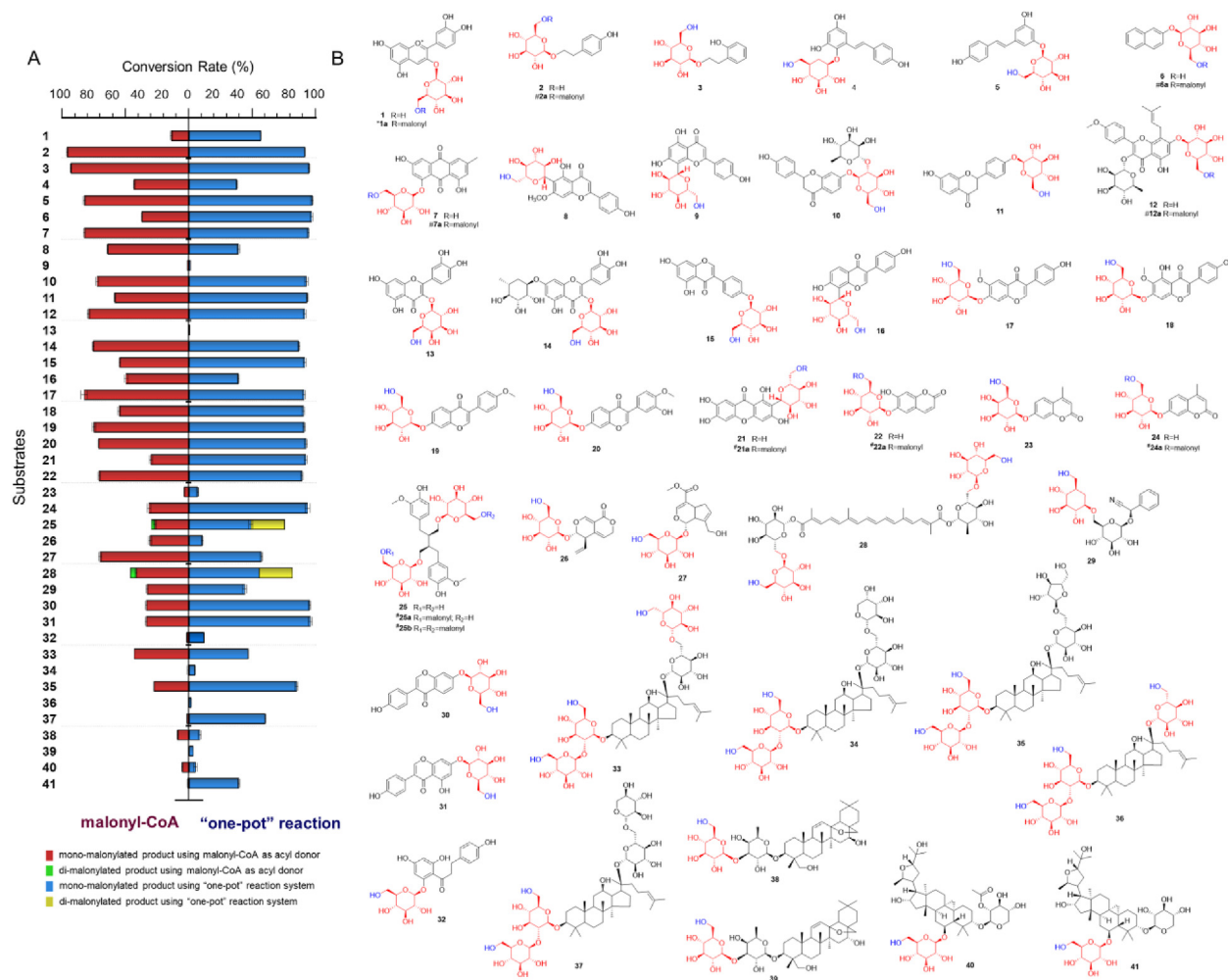


**Figure 3** CtMaT1 catalyzes the malonylation of diverse glycoside substrates. (A) Conversion rates (%) of malonylated products of 1–41, using MLC as acyl-donor (left) and using a “one-pot” cascade reaction system (right); (B) Chemical structures of substrates 1–41 and preparative malonylated products. “#” represents the products purified and identified by NMR; “\*” 1a was identified by comparing with reference standards.

is the first malonyltransferase that accepts all these structural types of substrates simultaneously.

Furthermore, the activity of most reported malonyltransferases was highly dependent on substrate structure and substitution modes<sup>20</sup>. In contrast, the malonylation activity of CtMaT1 towards diverse glycosides was not restricted by the substituted sugar types or substitution modes on the aglycone. As shown in Fig. 3B, the substrate range of CtMaT1 included flavonoid glycosides with glycosyl groups substituted at C-6 (8), C-7 (10, 17–20, 30, 31), and C-8 (9 and 16) positions on ring A, C-4' (11 and 15) position on ring B, and C-3 (13 and 14) position on ring C. Additionally, the glycosyl substitution forms in its accepting substrates consisted of both *O*-glucosides and *C*-glucosides (8, 9, 16, and 21). Moreover, mono-glycosides (e.g., 26 and 27), di-glycosides (e.g., 3, 12, and 25), and multi-glycosides (e.g., 28, 30–41) could all be recognized by CtMaT1. As for the sugar moiety types, CtMaT1 showed high selectivity towards glucosides. Substrates containing a galactosyl group (13 and 23) can also be accepted by CtMaT1, but the activity is relatively weak.

Notably, the malonylated products of several glycosides were reported to have important physiological functions or desired

druggabilities. As illustrated in Fig. 1A, the malonylated derivatives of substrates 1, 6, 30, and 31 exhibited important roles as natural pigments<sup>13,14</sup>, xenobiotic metabolism-related agents<sup>9,10</sup>, and effective anticancer candidates<sup>57</sup>, respectively. CtMaT1 showed desired malonylation activities towards these compounds, implying its application potential in synthesizing these bioactive molecules. Especially, CtMaT1 also displayed malonylation activity towards ginsenosides (33–37), saikosaponins (38–39), and astragalosides (40–41). These complex saponins are medicinally important saponins with a wide range of pharmacological activities. The enzymatic malonylation of these saponins has never been previously reported. Among them, malonyl ginsenosides are widely present in ginseng plants and possess significant hypoglycemic and antidiabetic effects<sup>58,59</sup>. The recognition of CtMaT1 towards these saponins further expands its substrate spectrum for natural products with complex structures while emphasizing its pharmaceutical usage significance.

Furthermore, CtMaT1 could also catalyze di-malonylation reactions. When using secoisolaricresinol diglucoside (25) as the substrate, two products (25a and 25b) were detected by HPLC–UV analyses (Fig. S31). They manifested a similar UV absorption

spectrum as **25**. The HRESI-MS spectra of **25a** and **25b** exhibited  $[M-H]^-$  ions at  $m/z$  771.2713 and  $m/z$  857.2757, respectively, indicating the formation of mono- and di-malonylated products with calculated molecular formulas of  $C_{35}H_{48}O_{19}$  and  $C_{38}H_{50}O_{22}$ . Similarly, a mono-malonylated product **28a** with the formula  $C_{47}H_{66}O_{27}$  ( $[M-H]^-$  ion at  $m/z$  1061.3741), and a di-malonylated product **28b** with the formula  $C_{50}H_{68}O_{30}$  ( $[M-2H]^{2-}$  ion at  $m/z$  573.1816) were both detected when using crocin (**28**) as a substrate (Fig. S34). This observation further confirmed the di-malonylation activity of CtMaT1 toward different glycosides.

Next, the acyl-donor selectivity of CtMaT1 was further assessed using methylmalonyl-CoA (methyl-MLC) as an acyl-donor. Trace products were detected for 19 tested substrates and identified as corresponding methylmalonyl products by HPLC and HRESI-MS analyses (Supporting Information Figs. S48–S66 and Table S6). The findings indicated that CtMaT1 is a highly specific malonyltransferase, and the utilization of both MLC and methyl-MLC has further expanded the catalytic scope of CtMaT1.

### 3.4. Establishment of a “one-pot” cascade system to efficiently biosynthesize diverse malonylated glycosides

Given the unprecedented catalytic tolerance, CtMaT1 has the potential to serve as a universal tool for versatile enzymatic malonylation. However, the commercial expense and chemical instability of the active acyl-donor MLC limit the further application of CtMaT1 to some extent. To address this issue, we amplified MatB (GenBank ID AY250842), which encodes an MLC synthetase, from *A. thaliana*<sup>30</sup> and expressed it heterologously in *E. coli* (Figs. S2 and S4). Successful production of MLC (Supporting Information Fig. S67, peak a) was made directly from malonic acid in the presence of CoA, ATP, and MatB proteins. In order to simplify the two sequential malonylation steps and prevent potential MLC degradation during application, a “one-pot” synthesis was developed. In this reaction assembly line, MLC was synthesized by MatB and utilized in situ in the malonylation step conducted by CtMaT1. Meanwhile, CoA could be regenerated and

recycled in the next circulation reaction after the malonyl group is released. Additionally, the consumption of acyl-donors can effectively shift the equilibrium towards end-product formation (Fig. 4A). HPLC–UV–ESI-MS analyses demonstrated that all the substrates depicted in Fig. 3B can be efficiently catalyzed within this “one-pot” reaction system, resulting in the formation of identical malonylated products with notable improvement in conversion rate for most compounds (Fig. 3A). Among them, products of **2**, **3**, **5–7**, **10–12**, **15**, **17–21**, **24**, **30** and **31** can reach a high conversion yield of more than 90% (Fig. 3 and Table S5).

Considering that MatB could also conduct the synthesis of methyl-MLC (Supporting Information Fig. S68, peak b), the “one-pot” reaction systems with methylmalonic acid, ATP, CoA, and all the above positive substrates were incubated. The corresponding methylmalonylated products were successfully detected in nineteen tested substrates (listed in Table S6) with a relatively low conversion yield, possibly due to the malonyltransferase specificity of CtMaT1 and the lower activity of MatB against methylmalonic acid<sup>30</sup>.

### 3.5. CtMaT1 catalyzes both mono- and di-malonylation with high regiospecificity at the C6-hydroxyl position of the glucose chain

To further investigate the catalytic properties of CtMaT1, scaled-up preparations of malonylated products were carried out using this “one-pot” synthesis system for eight representative substrates (**2**, **6**, **7**, **12**, **21**, **22**, **24**, and **25**) that belong to the PhGs (**2**), naphthalene glycoside (**6**), anthraquinone glycoside (**7**), flavonol glycoside (**12**), xanthone glycoside (**21**), coumarin glycoside (**24**), and lignan glycoside (**25**) respectively. The corresponding mono-malonylated products (**2a**, **6a**, **7a**, **12a**, **21a**, **22a**, **24a**, and **25a**), and one di-malonylated product **25b** (Fig. 4B) were obtained and structurally characterized as 6'-malonyl-salidroside (**2a**), 6'-malonyl-2-naphthyl-glucoside (**6a**), 6'-malonyl-emodin 8-*O*-glucoside (**7a**), 6'''-malonyl-icariin (**12a**), 6'-malonyl-mangiferin (**21a**), 6'-malonyl-esculin (**22a**), 6'-malonyl-4-methylumbelliferyl-glucoside (**24a**),

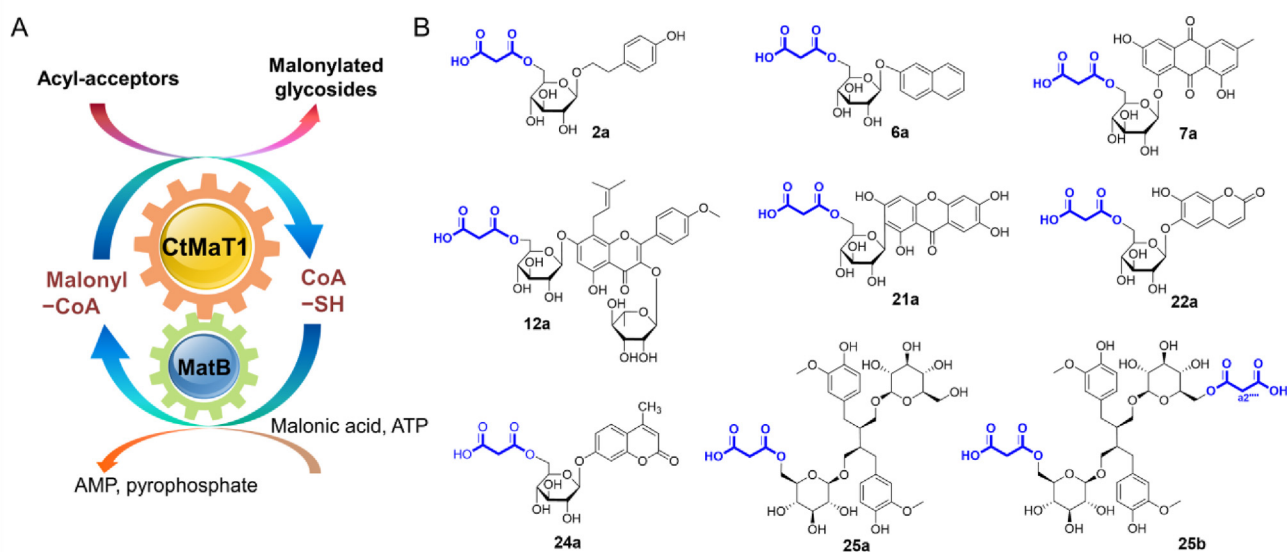


**Figure 4** Preparative-scale malonylation of different glycosides using “one-pot” reaction system (A) and the chemical structures of the prepared malonylated products **2a**, **6a**, **7a**, **12a**, **21a**, **22a**, **24a**, **25a**, and **25b** with malonyl group regiospecifically substituted at the C6 glycosyl hydroxy group of sugar unit (B).

6'''-malonyl-secoisolariciresinol diglucoside (**25a**) and 6''',a6'''-dimalonyl-secoisolariciresinol diglucoside (**25b**), respectively. These results demonstrated the exceptional catalytic regioselectivity of CtMaT1, as evidenced by its ability to specifically introduce malonyl groups at the 6-hydroxyl position of glucose moieties in all tested substrates during both mono- and di-malonylation reactions.

The extensive substrate tolerance of CtMaT1 toward various glucosides, coupled with its high regioselectivity toward the 6-OH group of the sugar unit, makes it an ideal enzymatic tool for achieving regioselective malonylation at the C6-hydroxy position of diverse glucosides. Moreover, to the best of our knowledge, CtMaT1 represents the first malonyltransferase that displays remarkable substrate promiscuity alongside catalytic regioselectivity.

### 3.6. Mono-malonylated glucosides **21a**, **25a**, and di-malonylated glucoside **25b** showed significant DPPH radical scavenging activity

The obtained nine new malonylated glycosides were evaluated for pharmacological activity using test models selected primarily based on the reported activities of the substrates. Interesting findings were obtained in the evaluation of free radical scavenging activity. Compounds **2a**, **21a**, **25a**, and **25b** as well as their unmodified types **2**, **21**, and **25** were assayed at 50  $\mu\text{mol/L}$  (final concentration) towards DPPH free radical with Trolox as the positive control. Interestingly, it was found that the percentages of scavenged DPPH radical of mono-malonylated glycosides **21a**, **25a**, and di-malonylated glycoside **25b** were  $81.90 \pm 0.5\%$ ,  $65.9 \pm 1.2\%$ , and  $67.5 \pm 1.1\%$  respectively, which were much higher than the positive control Trolox whose inhibition percentage was determined to be  $54.2 \pm 1.2\%$ . Furthermore, in comparison to their original counterparts **21** ( $71.1 \pm 0.2\%$ ) and **25** ( $53.8 \pm 0.1\%$ ), the introduction of the malonyl group resulted in an enhancement of bioactivities. DPPH radical scavenging activity could directly reflect the antioxidant potential of tested compounds<sup>60</sup>. The favorable DPPH radical scavenging abilities exhibited by **21a**, **25a**, and **25b** suggest their promising prospects for development into antioxidant agents.

### 3.7. AlphaFold2 protein structure prediction of CtMaT1 and structural basis for MLC recognition

The remarkable catalytic properties of CtMaT1 make it an intriguing subject for further investigation into the structural basis of its unusual catalysis characteristics. Unfortunately, the crystal structure of CtMaT1 failed to get after lots of effort. Therefore, the protein structure of CtMaT1 was predicted using AlphaFold2<sup>31</sup>. All residues in the model were evaluated to be within reasonably allowed regions with 95.5% located in the most favored areas (Supporting Information Fig. S69), confirming the high credibility of the structure.

Totally 11  $\alpha$ -helices and 18  $\beta$ -strands were found in the tertiary structure of CtMaT1 forming two  $\alpha/\beta$  mixed subdomains that interacted with each other (Fig. 5A and Supporting Information Fig. S70). The active binding pocket of the ligands was located at the interface of two subdomains running through the protein forming a long solvent channel as shown in Fig. 5B and C. The conserved DFGWG motif is far from the active pocket and may help to support the conformation maintenance of the protein. The H $\times$  $\times$ D motif and YFGNC motif are located beside the interface

and contribute to the establishment of the central solvent channel<sup>61</sup>.

To identify the crucial amino acids in acyl-donor recognition, we conducted molecular docking studies with MLC utilizing Dm3MaT3 (PDB ID: 2E1T) as the template structure for donor binding pocket search. The optimum model was subjected to molecular dynamics (MD) simulation and reached a stable state after 50 ns simulation (Supporting Information Fig. S71). The binding pocket of MLC was found to link to the central solvent channel (Fig. 5C). The key residues interacting with MLC are labeled in Fig. 5D. Most of them are hydrophilic amino acids including R40, H167, D171, K249, Q261, S263, S264, F265, D300, R304, N352, S380, G381, S382, and R384. Notably, a total of sixteen hydrogen-bond interactions were observed in the donor pocket of CtMaT1, as summarized in Fig. 5E, exceeding the number identified in Dm3MaT3 (fourteen hydrogen-bonding interactions were identified)<sup>61</sup>. In the MLC-binding model of CtMaT1, it was observed that the side chain of R40, the backbone N atom of G381, and the main-chain N atom of D300 could interact with the carboxyl oxygen atom of the malonyl group and pantothenate moiety of MLC through the formation of hydrogen bonds, respectively (Fig. 5D and E). Mutants R40A and D300A induce a significant reduction in the catalytic activity of CtMaT1 towards all tested substrates (>90%, Fig. 5I), providing bioactivity evidence for the irreplaceable roles of R40 and D300 in MLC acceptance. Mutant G381A resulted in obvious activity diminishment towards different substrates (>50%, Fig. 5I). Alanine-scanning mutagenesis of other residues in acyl-donor binding pocket, including D171, K249, S263, S264, F265 and S380, also lead to noticeable decreases in CtMaT1 catalytic activities (Fig. 5I), highlighting their important roles in MLC recognizing.

Additionally, to support the malonylation tolerance towards different glycosides, CtMaT1 was predicted to have a strong binding affinity with MLC. This hypothesis was confirmed by the MM/GBSA-based binding free energy calculation. The calculated binding free energy for MLC in the CtMaT1-MLC complex was  $-42.9515$  kcal/mol, with a significant contribution from electrostatic interaction ( $-229.9059$  kcal/mol, Fig. 5J). The electrostatic potential on the CtMaT1 surface and the electrostatic charges of MLC were subsequently analyzed using the APBS tool and RESP charge model in the Gaussian 09 package, respectively. CtMaT1 exhibits remarkable electropositivity in the MLC binding pocket (Fig. 5G), while the deprotonated MLC possesses dominant negative charges (Fig. 5H). This affords a reasonable explanation that the distribution of counter-charges could evoke an attractive potential field to enhance the binding affinity of MLC with CtMaT1. Furthermore, the per-residue contributions were also analyzed. Residues R40, F265, and G381 were found to have the highest impact on MLC binding (Fig. 5J). These results provide additional structural evidence for the crucial roles of R40 and G381 in CtMaT1's activity as demonstrated in the above-mentioned mutagenesis studies.

### 3.8. Structural insights into CtMaT1's substrate promiscuity, preference and malonylation regioselectivity

To explain the substrate tolerance of CtMaT1 toward various glycosides, we selected nine glycoside substrates with different aglycone skeletons, including salidroside (**2**), 2,3,5,4'-tetrahydroxystilbene-2-O-glucoside (**4**), 2-naphthyl-glucoside (**6**), emodin-8-O-glucoside (**7**), icariin (**12**), mangiferin (**21**), esculin (**22**), 4-methylumbelliferyl-7-O-glucoside (**24**), secoisolaricir

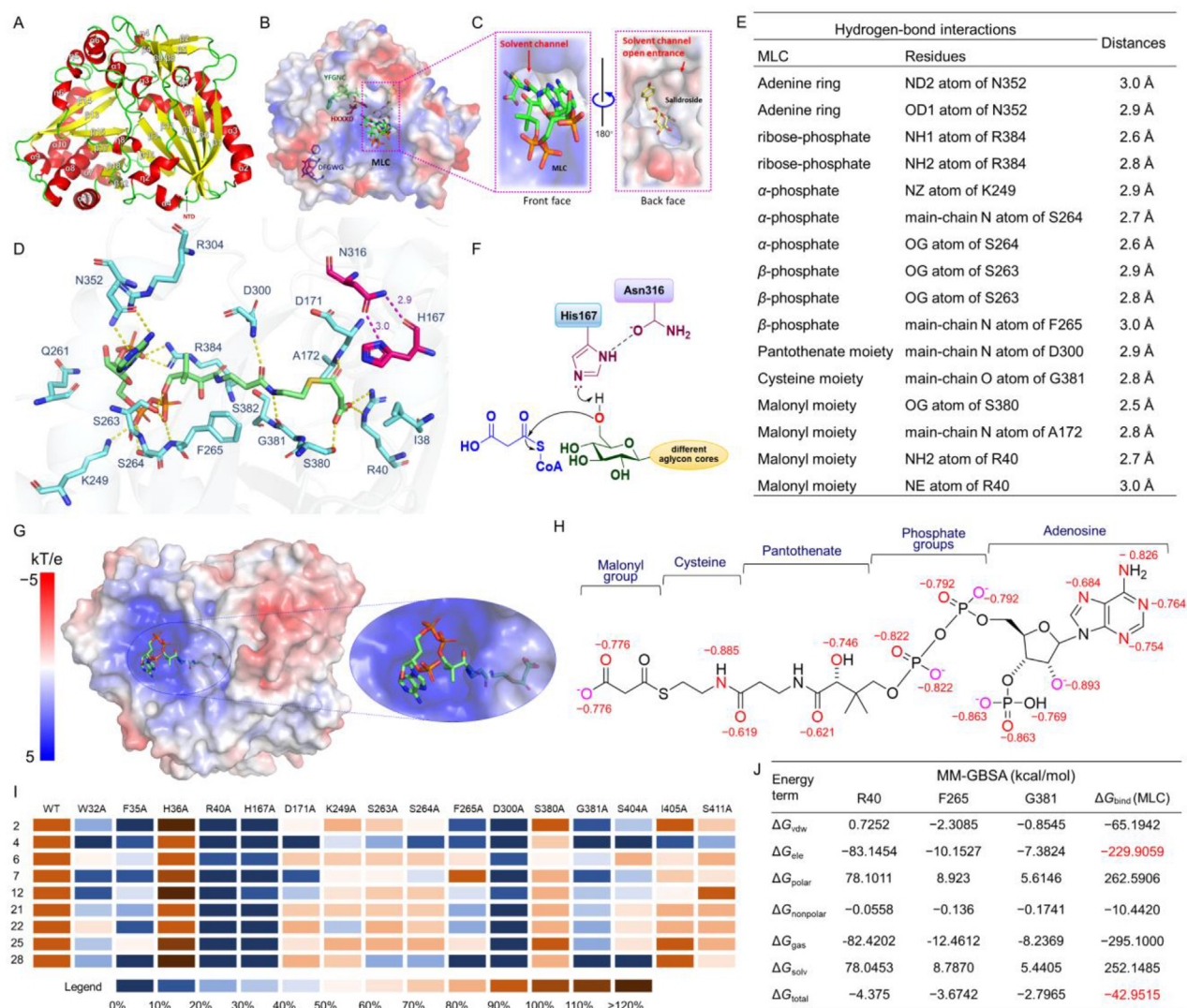


**Figure 5** Protein structure prediction, docking analysis, and mutagenesis studies of CtMaT1. (A) The overall structure of CtMaT1 in cartoon presentation with labeled secondary structure elements.  $\alpha$ -helices,  $\beta$ -sheets, and loops were shown in red, yellow, and green, respectively; (B) Surface presentation of CtMaT1 docking with MLC and salidroside highlights the conserved motifs of H $\times$  $\times$ D, DFGWG, and YFGNC which were shown as red sticks, blue sticks, and green sticks, respectively; (C) Magnified view of MLC binding pocket in the front face (left) and acyl-acceptor binding pocket at the back face (right) of CtMaT1 in surface presentation; (D) Docking results of key residues in MLC binding pocket. MLC and key residues are present as green and blue sticks, respectively. Hydrogen bonds between MLC and CtMaT1 are exhibited as yellow dashes; (E) Interaction details between MLC and key residues for acyl-donor recognition; (F)  $S_N2$  catalytic reaction mechanism of CtMaT1 conducted by residues H167 and N316; (G) Electrostatic potential of CtMaT1 surface. The electronegative zone, the neutral zone, and the electropositive zone are presented in red, white, and blue, respectively; (H) Calculated RESP-model charges of MLC. Atoms with negative charge values ( $<-0.6$ ) were labeled; (I) Site-directed mutagenesis study of CtMaT1 toward substrates **2**, **4**, **6**, **7**, **12**, **21**, **22**, **25**, and **28** using MLC as acyl-donor; (J) The MM/GBSA calculated binding free energy values for CtMaT1-MLC complex, and the decomposition energy values of the top three contributing residues.

esinol diglucoside (**25**), and crocin (**28**) as representative substrates for docking and dynamic simulation investigation. Docking results showed that the acyl-acceptor binding pocket is located on the back face of CtMaT1 and connects to the MLC binding pocket through the central solvent channel. This channel has a wide-open entrance (Fig. 5C) which effectively facilitates the entry of different substrates. Recently, an acetyltransferase AmAT7-3 that could utilize astragaloside IV (**41**) as an acetyl-acceptor was identified from *Astragalus membranaceus*<sup>62</sup>. In comparison with other reported acyltransferases, it possesses a remarkably enlarged

substrate pocket capable of accommodating the large-sized saponin molecule<sup>62</sup>. CtMaT1 exhibits a comparable substrate binding pocket with AmAT7-3 (PDB ID: 8H8I), which is significantly larger than those of SbHCT (PDB ID: 4KEC) and HCT (PDB ID: 5KJW) with known substrate binding pocket structures (Fig. 6A). Notably, the acyl-acceptor pocket of CtMaT1 displays adequate size in all three dimensions (Fig. 6J), making the inside pocket sufficiently capacious to accommodate a diverse range of glycoside substrates (left column in Fig. 6B–J) with varying aglycon cores of different sizes (Supporting Information Fig. S72).

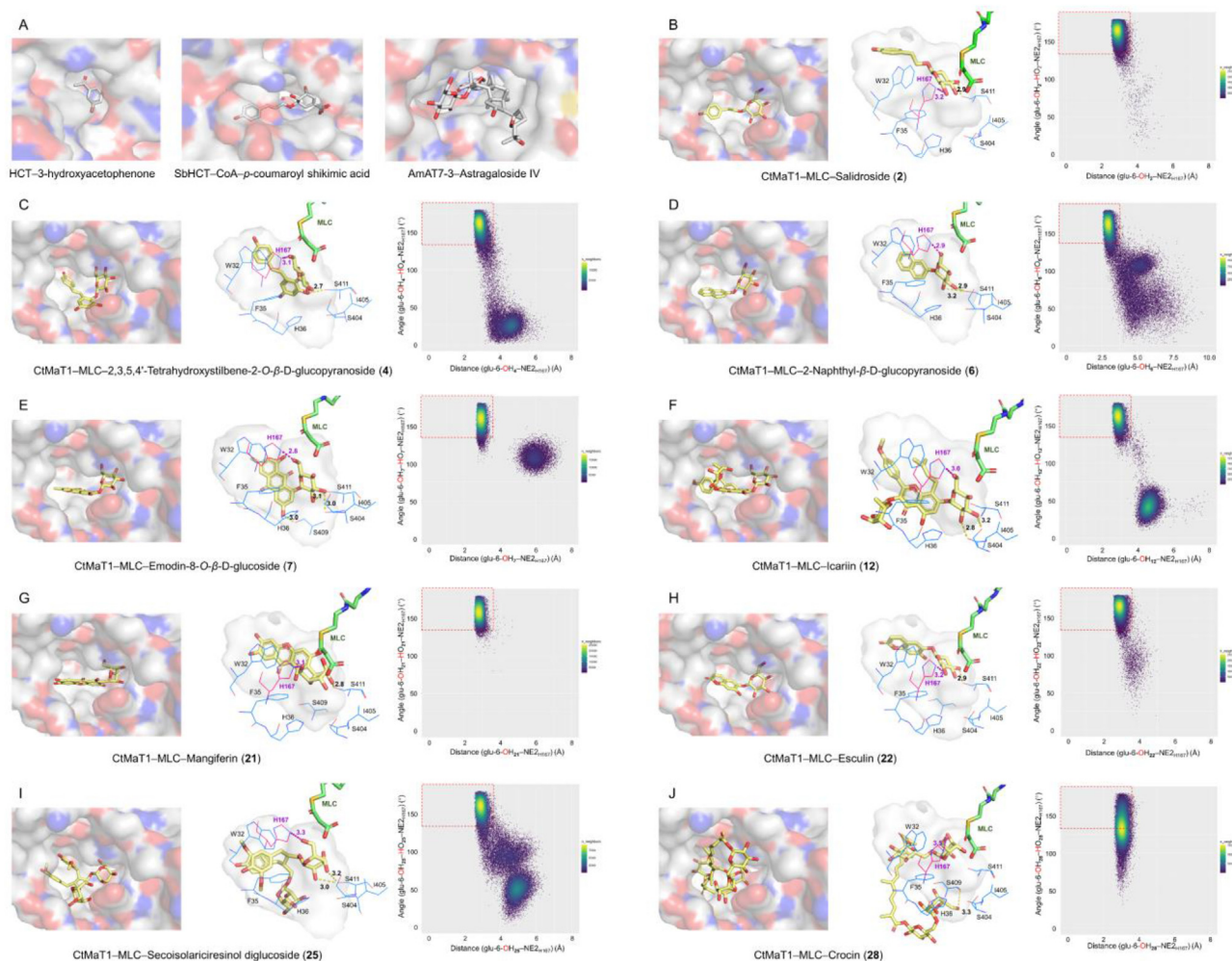


**Figure 6** (A) The substrate binding pocket surface of HCT, SbHCT, and AmAT7-3. (B–J) Representative conformations of different substrates (2, 4, 6, 7, 12, 21, 22, 25, and 28) in the acyl-acceptor binding site of CtMaT1 in surface view (left column), and the surrounded residues (middle column) and their corresponding conformation maps observed through MD simulations (right column). MLC and substrates are present as green and yellow sticks, respectively. The acyl-acceptor binding pocket shown as a white surface was computed and generated in PyMOL. The surrounding residues are shown in blue lines. H167 is shown as magenta lines. Hydrogen bonds are shown as dashes. The most populated conformations are shown in yellow and the least populated conformations are shown in blue in the maps produced by RStudio. The catalytic conformation region (defined as the distance between the glucose-6-hydroxyl-O of different substrates and the NE2 nitrogen of H167 is less than 3.6 Å and the angle of glucose-6-hydroxyl-O/glucose-6-hydroxyl-H/NE2 is larger than 135°)<sup>63</sup> is shown in a red box.

To probe the high malonylation regioselectivity of CtMaT1 on the 6-OH position of diverse substrates, we performed 50 ns simulations of nine “CtMaT1–MLC–substrate” complexes and analyzed the resulting trajectories (Supporting Information Fig. S73). The dominant conformation of each complex is shown in Fig. 6. Interestingly, regardless of the spatial geometry of the substrates, their sugar moieties are consistently positioned near the H167 residue. The imidazole functional group of H167 is found to be situated between the acyl-donor and acyl-acceptor pocket, and close to both the malonate moiety of MLC (Fig. 5D) and the glycosyl hydroxyl group of the glycoside substrates (Fig. 6). As a highly conserved catalytic residue in plant ATs, H167 was considered to act as a base catalyst to initiate the S<sub>N</sub>2 transfer reaction. Residue N316 (in the conserved YFGNC motif) also participates in this process and helps to stabilize the catalytic conformation and maintain the charge balance through hydrogen interactions with H167 (magenta dash in Fig. 5D).

Mutagenesis of H167 leads to a dramatic activity impairment towards all substrates (Fig. 5I), indicating its essential role in malonylation process. The representative conformations of the nine ternary complexes after dynamic simulation consistently revealed the formation of hydrogen bonds between H167 residue and the 6-OH group of glucose moiety in every case (middle column in Fig. 6B–J) and these interactions were highly stable during the whole simulation process (right column in Fig. 6B–J). Such conformations supported the transfer of malonyl moiety to the 6-OH position of the glucose moiety through the S<sub>N</sub>2 mechanism, thus giving a reasonable explanation for the regioselectivity of CtMaT1.

Furthermore, several other residues including W32, F35, H36, S404, I405, and S411 were also observed to be located close to the sugar moiety of various glycoside substrates to ensure the maintenance of the active conformation which supports catalysis (Fig. 6). Mutation of W32 or F35 to alanine both resulted in a

significant reduction in catalytic activity towards all tested substrates (Fig. 5I), demonstrating the crucial roles of these two residues in malonyltransferase activity for the first time. Their interactions will be discussed in Section 3.9. Mutations of S404, I405, and S411 to alanine resulted in noticeable decreases in enzymatic activity, indicating the participation of these residues in facilitating substrate recognition.

To further verify the above assumptions regarding the reaction mechanism of CtMaT1 and simultaneously investigate its preference for glucoside substrates, we carried out the QM/MM computation on two reaction models based on two isomeric compounds: 4-methylumbelliferyl- $\beta$ -D-galactopyranoside (**23**, MU-Gal) and 4-methylumbelliferyl- $\beta$ -D-glucopyranoside (**24**, MU-Glc), respectively (Supporting Information Fig. S74). Both **23** and **24** share the same aglycone with the only distinction lying in their sugar chains; specifically, **23** is a galactoside while **24** is a glucoside. The calculation result (Fig. 7A and B) demonstrated that the malonyl transfer process initiates by deprotonating the glycosyl hydroxyl unit. Furthermore, the successful detection of the tetrahedral intermediate (IM1, Fig. 7 and Fig. S74) between H167, MLC, and the substrate provides solid evidence for the predicted  $S_N2$  reaction mechanism conducted by H167. During the malonylation process, the imidazole ring of H167 initially

deprotonates the glycosyl hydroxyl unit of the glycoconjugate, generating a nucleophile that subsequently attacks the thioester bond of MLC and facilitates the transfer of the malonyl unit to the acyl-acceptor (Fig. 5F and Fig. S74). Additionally, the calculated free energy profiles for MU-Gal and MU-Glc complexes are depicted in Fig. 7C and D respectively. It is evident that the energy barriers for TS1 (37.80 kJ/mol) and TS2 (6.38 kJ/mol) of the MU-Glc complex were lower than that of the MU-Gal complex (41.57 and 10.89 kJ/mol, respectively). These results indicated that the malonyl transfer process of MU-Glc by deprotonating the glycosyl hydroxyl unit is much easier than that of MU-Gal, which is consistent with the experimental observations highlighting CtMaT1's pronounced preference towards glucosides.

### 3.9. Analysis of molecular mechanism underlying the increased di-malonylation activity of H36A

From the mutagenesis study, it was inspiring to obtain a mutant H36A that could largely increase the formation of the di-malonylation products. As shown in Fig. 8A and B, the conversion yield of di-malonylation product of **25** or **28** catalyzed by H36A increased 3–4 times compared to the wild-type CtMaT1. To elucidate the mechanism underlying the enhanced di-

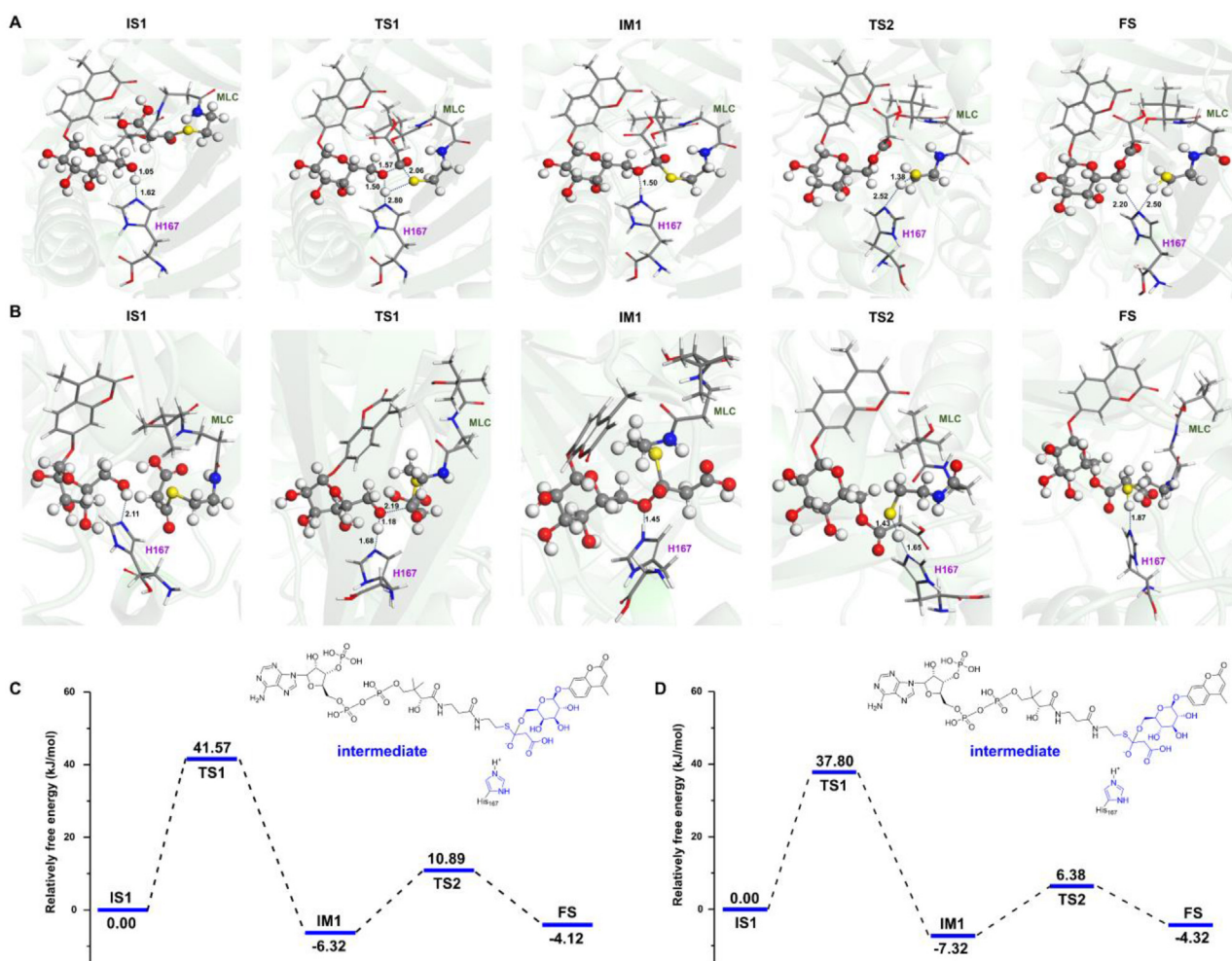


**Figure 7** (A, B) QM/MM-optimized reaction states of the malonylation of **23** (MU-Gal, A) and **24** (MU-Glc, B) by CtMaT1. (C, D) Calculated energy profiles for CtMaT1–MLC–**23** ternary complex (C) and CtMaT1–MLC–**24** ternary complex (D). Energies are present in kJ/mol. (IS = initial state, TS = transition state, IM = intermediate, FS = final state.)

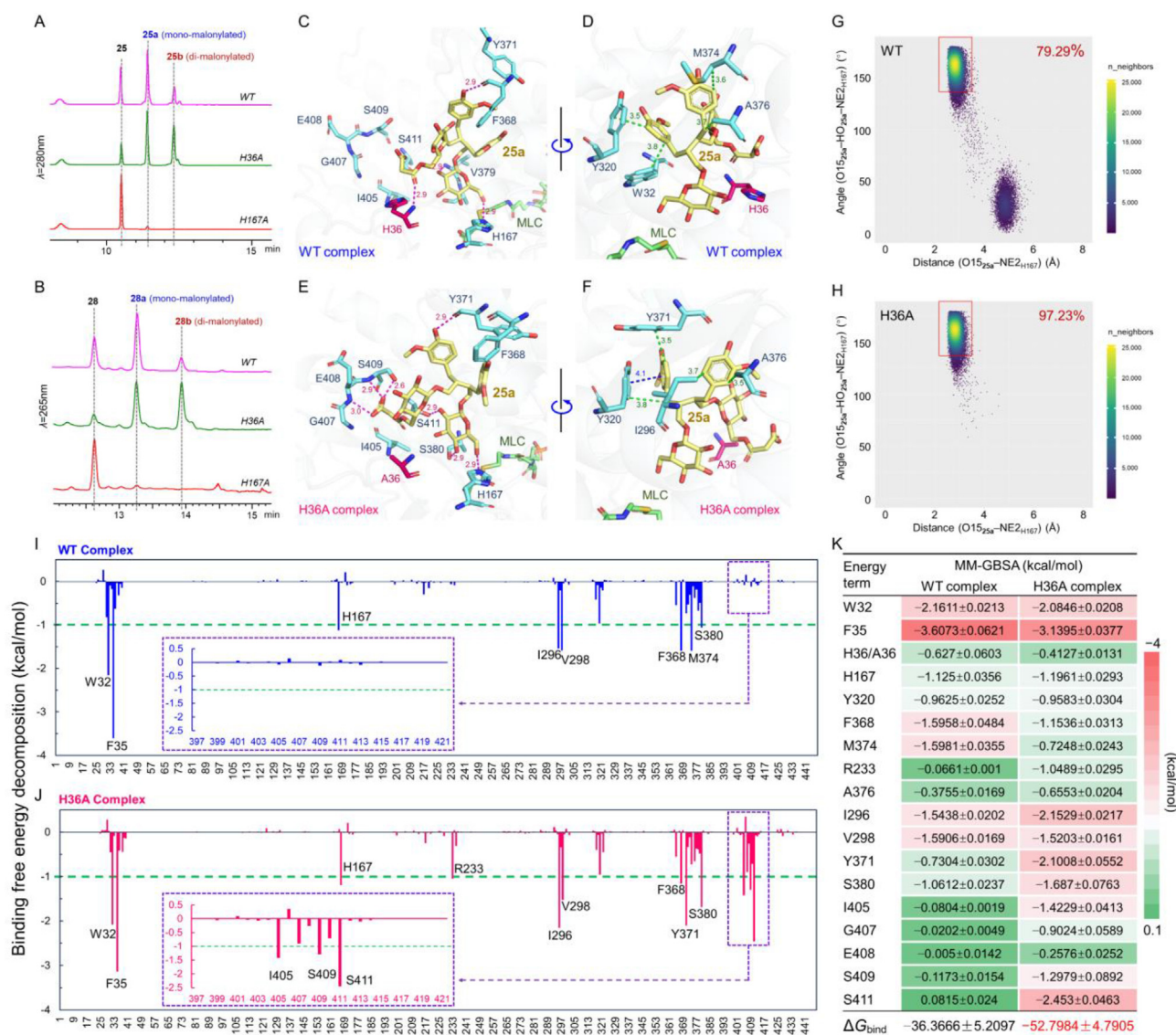


**Figure 8** Molecular mechanism underlying the increased di-malonylation activity of CtMaT1. (A, B) HPLC chromatograms of mono- and di-malonylation reactions of substrates **25** (A) and **28** (B) catalyzed by wild-type (WT) CtMaT1, mutants H36A and H167A, respectively; (C–F) Representative ternary complex of WT–MLC–**25a** (C, D) and H36A–MLC–**25a** (E, F) in MD simulations, respectively. Substrate **25a** is shown as yellow sticks. The interacted residues are shown as cyan sticks. Residues H36 or A36 are shown as magenta sticks. Hydrogen interactions, hydrophobic interactions, and  $\pi$ -stacking interactions are labeled as magenta, green, and blue dashes, respectively; (G, H) Conformation maps of WT–MLC–**25a** complex (G) and H36A–MLC–**25a** complex (H) during MD simulation processes. The most populated conformations are shown in yellow and the least populated conformations are shown in blue. The catalytic conformation region is shown in a red box; (I, J) Per-residue binding free energy contribution profiles of WT complex (I) and H36A complex (J). The residue region around 397 to 421 was magnified. Residues contributing more than  $-1.00$  kcal/mol binding free energy are marked; (K) The MM/GBSA calculated binding free energy values for WT complex and H36A complex, and the decomposition energy values of the involved key residues.

malonylation activity of H36A, we employed the mono-malonylated product **25a** as an acyl-acceptor and subsequently established the ternary complex of CtMaT1<sub>WT</sub>–MLC–**25a** (WT complex) and CtMaT1<sub>H36A</sub>–MLC–**25a** (H36A complex) for MD simulation. After a 50 ns simulation, the predominate conformations of **25a** in the WT complex and H36A complex are shown in Fig. 8C–F, respectively. In the WT complex, in addition to the hydrogen bond between H167 and  $\alpha$ 6''-OH of glucose moiety that exists in both complexes and directly conducts the malonylation reaction, three additional hydrogen bonds (between **25a** and

residues H36, F368 and V379) (Fig. 8C) and four hydrophobic interactions (between **25a** and residues W32, Y320, M374 and A376) (Fig. 8D) were observed. However, when histidine 36 was replaced by alanine, the hydrogen bond between the carboxyl oxygen atom of the malonyl moiety of **25a** and the H36 residue was disrupted. Meanwhile, more spatial spaces will be provided for **25a** binding that will cause a conformation change of **25a** thus leading to the formation of six new hydrogen interactions with residues G407, E408, S409, Y371, S380, and S411 (Fig. 8E). Besides, four hydrophobic interactions (between **25a** and residues

I296, Y320, Y371, and A376) and a  $\pi$ -stacking interaction (between **25a** and Y320) were also observed in H36A complex (Fig. 8F). These interactions effectively contribute to substrate stabilization and facilitate the di-malonylation reaction, as supported by further analysis of MD trajectory. The emergence frequencies of catalysis-conformation (refined as the distance between the active site  $a6'''$ -OH and catalysis H167<sub>NE2</sub> atom  $\leq 3.6$  Å meanwhile the angle of H167<sub>NE2</sub> atom/ $a6'''$ -OH-H/ $a6'''$ -OH-O  $\geq 135^\circ$ )<sup>63</sup> in WT complex and H36A complex were calculated, respectively. The catalysis-conformation emergence frequency of the H36A complex was 97.23% (Fig. 8H), which was much higher than that of the WT complex at 79.29% (Fig. 8G).

To provide more insights into the improved di-malonylation activity of mutant H36A, the binding free energy of the catalytic conformations of WT complex and H36A complex, as well as the per-residue binding energy contribution, were calculated by the MM/GBSA approach, respectively<sup>64</sup>. The binding energy profiles of each residue in the WT complex (Fig. 8I) and H36A complex (Fig. 8J) showed a high degree of similarity across most regions, with notable changes observed around residues I405 to S411, which had moderate energy contributions in the WT complex (Fig. 8I). However, in the H36A complex, notable energy contributions were made by I405, G407, S409 and S411 with values of  $-1.4229$ ,  $-0.9024$ ,  $-1.2979$  and  $-2.4530$  kcal/mol, respectively (Fig. 8J). This corresponded with the above observed conformation change of **25a** in the H36A complex which leads to the new interactions between **25a** and residue region encompassing I405 to S411. Additionally, the newly engaged hydrogen interaction between **25a** and Y371 was also confirmed by a higher decomposition binding free energy value of Y371 ( $-2.1008$  kcal/mol) compared to that in the WT complex ( $-0.7304$  kcal/mol). Finally, the total binding free energy of the catalytic conformations of WT complex and H36A complex were determined to be  $-36.3666$  and  $-52.7984$  kcal/mol, respectively (Fig. 8K). The decreased binding free energy observed in the H36A complex provides stronger evidence for the enhanced di-malonylation activity of the mutant.

Another noteworthy finding is that W32 and F35 make the most important contributions to the binding energy of both the WT complex and H36A complex (Fig. 8I), which is primarily attributed to their favorable van der Waals interactions (Supporting Information Table S7). This observation aligns with previous findings that W32 and F35 are located nearby the sugar moiety of various glycoside substrates (Fig. 6), as well as the mutagenesis results that mutating W32 and F35 to alanine leads to a substantial catalysis activity collapse (Fig. 8I), thus further confirming their crucial roles in malonylation process from a binding free energy perspective.

#### 4. Conclusions

In this work, a new malonyltransferase CtMaT1 with both unprecipitated substrate promiscuity and high malonylation regiospecificity was identified from the herb *C. tubulosa*. Its substrate spectrum covered a majority of the common types of natural glycosides possessing different kinds of aglycon and the malonyl groups were specifically introduced into the at the C6-hydroxyl position of the glucose chain. Nine new malonylated glycosides were effectively synthesized using a one-pot reaction system and three of them demonstrated considerable DPPH radical scavenging activities. The structural insights into these unusual catalytic characteristics of CtMaT1 were explored. CtMaT1 showed a high binding affinity with the acyl-donor MLC through hydrogen and

electrotactic interactions. R40, D300, and G381 were identified to be critical in MLC recognition. A sufficiently large acyl-acceptor pocket with a widely opened entrance was observed in CtMaT1, which enables its remarkable substrate promiscuity to accommodate a diverse range of glycosides. Stable hydrogen bonds between the glucose-6-OH group in tested substrates and residue H167 functioned as the general base catalyst to initiate the deprotonation determined the regiospecific malonyl transfer to the C6-glycosyl hydroxy group. W32 and F35 helped to maintain the catalysis conformations through van der Waals interactions. QM/MM calculation confirmed the  $S_N2$  reaction mechanism of CtMaT1 and found that the energy barrier for the transition state of glucoside was lower than that of the galactoside, demonstrating the preference of CtMaT1 toward glucosides. Additionally, a mutant H36A exhibiting significantly enhanced di-malonylation activity was obtained. The underlying molecular mechanism proposed an intriguing model wherein single-site mutagenesis can initiate the conformational change of the mono-malonylated substrate, thereby facilitating newly established interactions between the ligand and the protein and leading to enhanced production of di-malonylation products. Our research provides an ideal plant malonyltransferase with both substrate promiscuity and catalysis regiospecificity to be used as a versatile tool for the malonylation of different glycosides to explore new bioactive compounds. The results also greatly expanded the understanding of plant acyltransferases from both functional and protein structural perspectives.

#### Acknowledgments

This work was financially supported by National Key Research and Development Program Special Project of Synthetic Biology (Grant No. 2023YFA0914100/2023YFA0914103), National Natural Science Foundation of China (Grant No. 82173922, 81402809), Beijing Natural Science Foundation (Grant No. 7192112), Fundamental Research Funds for the Central Universities (Grant No. 2023-JYB-JBQN-054, China), Young Elite Scientists Sponsorship Program by CAST (Grant No. CACM-2018-QNRC1-02, China), and State Key Laboratory of Natural and Biomimetic Drugs Foundation (Grant No. K202119, China).

#### Author contributions

Pengfei Tu, Shepo Shi, Jun Li, and Xiao Liu designed the research; Yuyu Liu, Xiping Xu, Wenqian Huang, Xiao Liu, Yaru Yan, Yingxia Wang, Weisheng Tian, Ting Mo, and Xiaoxue Cui performed the research. Xiao Liu analyzed data and wrote the paper; Shepo Shi, Jun Li, and Pengfei Tu revised the paper.

#### Conflicts of interest

The authors declare no conflict of interest.

#### Appendix A. Supporting information

Supporting data to this article can be found online at <https://doi.org/10.1016/j.apsb.2024.02.007>.

#### References

1. Newman DJ, Cragg GM, Snader KM. Natural products as sources of new drugs over the period 1981–2002. *J Nat Prod* 2003;**66**:1022–37.

- Weymouth-Wilson AC. The role of carbohydrates in biologically active natural products. *Nat Prod Rep* 1997;**14**:99–110.
- González-Sabín J, Morán-Ramallal R, Rebollo F. Regioselective enzymatic acylation of complex natural products: expanding molecular diversity. *Chem Soc Rev* 2011;**40**:5321–35.
- Suzuki H, Nakayama T, Yonekura-Sakakibara K, Fukui Y, Nakamura N, Yamaguchi MA, et al. cDNA cloning, heterologous expressions, and functional characterization of malonyl-coenzyme a: anthocyanidin 3-O-glucoside-6"-O-malonyltransferase from dahlia flowers. *Plant Physiol* 2002;**130**:2142–51.
- Zhao CL, Yu YQ, Chen ZJ, Wen GS, Wei FG, Zheng Q, et al. Stability-increasing effects of anthocyanin glycosyl acylation. *Food Chem* 2017;**214**:119–28.
- Lin Y, Li C, Shao P, Jiang L, Chen B, Farag MA. Enzymatic acylation of cyanidin-3-O-glucoside in raspberry anthocyanins for intelligent packaging: improvement of stability, lipophilicity and functional properties. *Curr Res Food Sci* 2022;**5**:2219–27.
- Li J, Halitschke R, Li D, Paetz C, Su H, Heiling S, et al. Controlled hydroxylations of diterpenoids allow for plant chemical defense without autotoxicity. *Science* 2021;**371**:255–60.
- Heiling S, Schuman MC, Schoettner M, Mukerjee P, Berger B, Schneider B, et al. Jasmonate and ppHsystemin regulate key malonylation steps in the biosynthesis of 17-hydroxygeranylinalool diterpene glycosides, an abundant and effective direct defense against herbivores in *Nicotiana attenuata*. *Plant Cell* 2010;**22**:273–92.
- Taguchi G, Ubukata T, Nozue H, Kobayashi Y, Takahi M, Yamamoto H, et al. Malonylation is a key reaction in the metabolism of xenobiotic phenolic glucosides in *Arabidopsis* and tobacco. *Plant J* 2010;**63**:1031–41.
- Taguchi G, Shitchi Y, Shirasawa S, Yamamoto H, Hayashida N. Molecular cloning, characterization, and downregulation of an acyltransferase that catalyzes the malonylation of flavonoid and naphthol glucosides in tobacco cells. *Plant J* 2005;**42**:481–91.
- Gan S, Rozhon W, Varga E, Halder J, Berthiller F, Poppenberger B. The acyltransferase PMAT1 malonylates brassinolide glucoside. *J Biol Chem* 2021;**296**:100424.
- Noda N, Yoshioka S, Kishimoto S, Nakayama M, Douzono M, Tanaka Y, et al. Generation of blue chrysanthemums by anthocyanin B-ring hydroxylation and glucosylation and its coloration mechanism. *Sci Adv* 2017;**3**:e1602785.
- Suzuki H, Nakayama T, Yonekura-Sakakibara K, Fukui Y, Nakamura N, Nakao M, et al. Malonyl-CoA: anthocyanin 5-O-glucoside-6"-O-malonyltransferase from scarlet sage (*Salvia splendens*) flowers. Enzyme purification, gene cloning, expression, and characterization. *J Biol Chem* 2001;**276**:49013–9.
- Yamazaki M, Gong Z, Fukuchi-Mizutani M, Fukui Y, Tanaka Y, Kusumi T, et al. Molecular cloning and biochemical characterization of a novel anthocyanin 5-O-glucosyltransferase by mRNA differential display for plant forms regarding anthocyanin. *J Biol Chem* 1999;**274**:7405–11.
- Jokioja J, Yang B, Linderborg KM. Acylated anthocyanins: a review on their bioavailability and effects on postprandial carbohydrate metabolism and inflammation. *Compr Rev Food Sci Food Saf* 2021;**20**:5570–615.
- Mellou F, Lazari D, Skaltsa H, Tselepis AD, Kolisis FN, Stamatis H. Biocatalytic preparation of acylated derivatives of flavonoid glycosides enhances their antioxidant and antimicrobial activity. *J Biotechnol* 2005;**116**:295–304.
- Xin X, Zhang M, Li X, Lai F, Zhao G. Biocatalytic synthesis of acylated derivatives of troxerutin: their bioavailability and antioxidant properties *in vitro*. *Microb Cell Fact* 2018;**17**:130.
- Oliveira H, Perez-Gregório R, de Freitas V, Mateus N, Fernandes I. Comparison of the *in vitro* gastrointestinal bioavailability of acylated and non-acylated anthocyanins: purple-fleshed sweet potato vs red wine. *Food Chem* 2019;**276**:410–8.
- D'Auria JC. Acyltransferases in plants: a good time to be BAHD. *Curr Opin Plant Biol* 2006;**9**:331–40.
- Bontpart T, Cheynier V, Ageorges A, Terrier N. BAHD or SCPL acyltransferase? What a dilemma for acylation in the world of plant phenolic compounds. *New Phytol* 2015;**208**:695–707.
- Riva S. Enzymatic modification of the sugar moieties of natural glycosides. *J Mol Catal B Enzym* 2002;**19**:43–54.
- Citterio A, Santi R, Fiorani T, Strologo S. Oxidation of malonic acid derivatives by manganese (III) acetate. Aromatic malonylation reaction. Scope and limitations. *J Org Chem* 1989;**54**:2703–12.
- Saito K, Yamazaki M. Biochemistry and molecular biology of the late-stage biosynthesis of anthocyanin: lessons from *Perilla frutescens* as a model plant. *New Phytol* 2002;**155**:9–23.
- Riva S, Danieli B, Luisetti M. A two-step efficient chemoenzymatic synthesis of flavonoid glycoside malonates. *J Nat Prod* 1996;**59**:618–21.
- Wang LL, Chen K, Zhang M, Ye M, Qiao X. Catalytic function, mechanism, and application of plant acyltransferases. *Crit Rev Biotechnol* 2021;**20**:1–20.
- Kogawa K, Kazuma K, Kato N, Noda N, Suzuki M. Biosynthesis of malonylated flavonoid glycosides on the basis of malonyltransferase activity in the petals of *Clitoria ternatea*. *J Plant Physiol* 2007;**164**:886–94.
- Jiang Y, Tu PF. Analysis of chemical constituents in *Cistanche* species. *J Chromatogr A* 2009;**1216**:1970–9.
- Yan Y, Mo T, Huang W, Xu X, Tian W, Wang Y, et al. Glycosylation of aromatic glycosides by a promiscuous glycosyltransferase UGT71BD1 from *Cistanche tubulosa*. *J Nat Prod* 2022;**85**:1826–36.
- Kumar S, Stecher G, Li M, Knyaz C, Tamura K, MEGA X. Molecular evolutionary genetics analysis across computing platforms. *Mol Biol Evol* 2018;**35**:1547–9.
- Chen H, Kim HU, Weng H, Browse J. Malonyl-CoA synthetase, encoded by acyl activating enzyme13, is essential for growth and development of *Arabidopsis*. *Plant Cell* 2011;**23**:2247–62.
- Jumper J, Evans R, Pritzel A, Green T, Figurnov M, Ronneberger O, et al. Highly accurate protein structure prediction with AlphaFold. *Nature* 2021;**596**:583–9.
- Laskowski RA, MacArthur MW, Moss DS, Thornton JM. PROCHECK: a program to check the stereochemical quality of protein structures. *J Appl Crystallogr* 1993;**26**:283–91.
- Trott O, Olson AJ. AutoDock Vina: improving the speed and accuracy of docking with a new scoring function, efficient optimization, and multithreading. *J Comput Chem* 2010;**31**:455–61.
- McLean AD, Chandler GS. Contracted Gaussian-basis sets for molecular calculations. *J Chem Phys* 1980;**72**:5639–48.
- Tian C, Kasavajhala K, Belfon KA, Raguet L, Huang H, Miguels AN, et al. ff19SB: amino-acid-specific protein backbone parameters trained against quantum mechanics energy surfaces in solution. *J Chem Theory Comput* 2019;**16**:528–52.
- Becke A. Density-functional thermochemistry. III. The role of exact exchange. *J Chem Phys* 1993;**98**:5648–52.
- Lee C, Yang W, Parr RG. Development of the Colle-Salvetti correlation-energy formula into a functional of the electron density. *Phys Rev B* 1988;**37**:785–9.
- Bayly CI, Cieplak P, Cornell WD, Kollman PA. A well-behaved electrostatic potential based method using charge restraints for deriving atomic charges: the RESP model. *J Phys Chem* 1993;**97**:10269–80.
- Mark P, Nilsson L. Structure and dynamics of the TIP3P, SPC, and SPC/E water models at 298 K. *J Phys Chem A* 2001;**105**:9954–60.
- Miller III BR, McGee Jr TD, Swails JM, Homeyer N, Gohlke H, Roitberg AE. MMPBSA.py: an efficient program for end-state free energy calculations. *J Phys Chem* 1993;**97**:10269–80.
- Frisch MJ, Trucks GW, Schlegel HB, Scuseria GE, Robb MA, Cheeseman JR, et al. Gaussian 09W, revision A.02. Gaussian, Inc., Wallingford CT, USA, 2009.
- Ditchfield R, Hehre WJ, Pople JA. Self-consistent molecular-orbital methods. IX. An extended Gaussian-type basis for molecular-orbital studies of organic molecules. *J Chem Phys* 1971;**54**:724–8.
- Rappé AK, Casewit CJ, Colwell K, Goddard III WA, Skiff WM. UFF, a full periodic table force field for molecular mechanics and molecular dynamics simulations. *J Am Chem Soc* 1992;**114**:10024–35.

44. St-Pierre B, De Luca V. Origin and diversification of the BAHD superfamily of acyltransferases involved in secondary metabolism. *Recent Adv Phytochem* 2000;**34**:285–315.
45. Yonekura-Sakakibara K, Tanaka Y, Fukuchi-Mizutani M, Fujiwara H, Fukui Y, Ashikari T, et al. Molecular and biochemical characterization of a novel hydroxycinnamoyl-CoA: anthocyanin 3-*O*-glucoside-6''-*O*-acyltransferase from *Perilla frutescens*. *Plant Cell Physiol* 2000;**41**:495–502.
46. Manjasetty BA, Yu XH, Panjekar S, Taguchi G, Chance MR, Liu CJ. Structural basis for modification of flavonol and naphthol glucosylconjugates by *Nicotiana tabacum* malonyltransferase (NtMaT1). *Planta* 2012;**236**:781–93.
47. Liu Y, Wang X, Mo T, Yan Y, Song Y, Zhao Y, et al. Identification and functional application of a new malonyltransferase NbMaT1 towards diverse aromatic glycosides from *Nicotiana benthamiana*. *RSC Adv* 2017;**7**:21028–35.
48. Suzuki H. cDNA cloning and functional characterization of flavonol 3-*O*-glucoside-6''-*O*-malonyltransferases from flowers of *Verbena hybrida* and *Lamium purpureum*. *J Mol Catal B Enzym* 2004;**28**:87–93.
49. Tropper M, Höhn S, Wolf L-S, Fritsch J, Kastner-Detter N, Rieck C, et al. 21-Hydroxypregnane 21-*O*-malonylation, a crucial step in cardenolide biosynthesis, can be achieved by substrate-promiscuous BAHD-type phenolic glucoside malonyltransferases from *Arabidopsis thaliana* and homolog proteins from *Digitalis lanata*. *Phytochemistry* 2021;**187**:112710.
50. Lopes D, Dettmann J, Nimalaratne C, Schieber A. Characterization and quantification of polyphenols in Amazon grape (*Pourouma cecropiifolia* Martius). *Molecules* 2010;**15**:8543–52.
51. Kikuchi N, Kwon YD, Gotoh M, Narimatsu H. Comparison of glycosyltransferase families using the profile hidden Markov model. *Biochem Biophys Res Commun* 2003;**310**:574–9.
52. Zhang M, Li FD, Li K, Wang ZL, Wang YX, He JB, et al. Functional characterization and structural basis of an efficient di-*C*-glycosyltransferase from *Glycyrrhiza glabra*. *J Am Chem Soc* 2020;**142**:3506–12.
53. Chen D, Chen R, Wang R, Li J, Xie K, Bian C, et al. Probing the catalytic promiscuity of a regio- and stereospecific *C*-glycosyltransferase from *Mangifera indica*. *Angew Chem Int Ed Engl* 2015;**54**:12678–82.
54. Chen R, Gao B, Liu X, Ruan F, Zhang Y, Lou J, et al. Molecular insights into the enzyme promiscuity of an aromatic prenyltransferase. *Nat Chem Biol* 2017;**13**:226–34.
55. Guo J, Ma X, Cai Y, Ma Y, Zhan Z, Zhou YJ, et al. Cytochrome P450 promiscuity leads to a bifurcating biosynthetic pathway for tanshinones. *New Phytol* 2016;**210**:525–34.
56. Sun Q, Huang M, Wei Y. Diversity of the reaction mechanisms of SAM-dependent enzymes. *Acta Pharm Sin B* 2021;**11**:632–50.
57. Koirala N, Pandey RP, Van Thang D, Jung HJ, Sohng JK. Glycosylation and subsequent malonylation of isoflavonoids in *E. coli*: strain development, production and insights into future metabolic perspectives. *J Ind Microbiol Biot* 2014;**41**:1647–58.
58. Liu Z, Li W, Li X, Zhang M, Chen L, Zheng YN, et al. Antidiabetic effects of malonyl ginsenosides from *Panax ginseng* on type 2 diabetic rats induced by high-fat diet and streptozotocin. *J Ethnopharmacol* 2013;**145**:233–40.
59. Liu Z, Wang LJ, Li X, Hu JN, Chen Y, Ruan CC, et al. Hypoglycemic effects of malonyl-ginsenosides extracted from roots of *Panax ginseng* on streptozotocin-induced diabetic mice. *Phytother Res* 2009;**23**:1426–30.
60. Sharma OP, Bhat TK. DPPH antioxidant assay revisited. *Food Chem* 2009;**113**:1202–5.
61. Unno H, Ichimaida F, Suzuki H, Takahashi S, Tanaka Y, Saito A, et al. Structural and mutational studies of anthocyanin malonyltransferases establish the features of BAHD enzyme catalysis. *J Biol Chem* 2007;**282**:15812–22.
62. Wang L, Jiang Z, Zhang J, Chen K, Zhang M, Wang Z, et al. Characterization and structure-based protein engineering of a regiospecific saponin acetyltransferase from *Astragalus membranaceus*. *Nat Commun* 2023;**14**:5969.
63. Li J, Yang J, Mu S, Shang N, Liu C, Zhu Y, et al. Efficient *O*-glycosylation of triterpenes enabled by protein engineering of plant glycosyltransferase UGT74AC1. *ACS Catal* 2020;**10**:3629–39.
64. Salomon-Ferrer R, Case DA, Walker RC. An overview of the Amber biomolecular simulation package. *Wiley Interdiscip Rev Comput Mol Sci* 2013;**3**:198–210.